THE ASTROPHYSICAL JOURNAL, 563:301–312, 2001 December 10

LONG-TERM MULTIWAVELENGTH OBSERVATIONS OF GRS 1758−258 AND THE ADVECTION-DOMINATED ACCRETION FLOW MODEL

JOHN W. KECK,[1] WILLIAM W. CRAIG,[2] CHARLES J. HAILEY,[1] FIONA HARRISON,[3] JAE SUB HONG,[1] STEVEN M. KAHN,[1] PHILIP M. LUBIN,[4] RYAN MCLEAN,[1] MICHAEL J. PIVOVAROFF,[1] MICHAEL SEIFFERT,[5] RON WURTZ,[2] AND KLAUS P. ZIOCK[2]

Received 2001 March 23; accepted 2001 August 8

ABSTRACT

We present a long-term multiwavelength light curve of Galactic black hole candidate GRS 1758−258 by combining previously published and archival data from *Granat*, *ROSAT*, the *Compton Gamma Ray Observatory*, the *Rossi X-Ray Timing Explorer*, *BeppoSAX*, *ASCA*, *EXOSAT*, and the Very Large Array. In addition, we include the first spectral results from the balloon-borne *Gamma-Ray Arcminute Telescope Imaging System* (*GRATIS*). In light of divergent analyses of the 1991–1993 *ROSAT* observations, we have reanalyzed these data; we find that the soft X-rays track the hard X-rays and that the fits require no blackbody component—indicating that GRS 1758−258 did not go to the high state in 1993. We offer an interpretation of these long-baseline data based on the advection-dominated accretion flow (ADAF) model for a system with $\dot{m} \lesssim \dot{m}_{\rm crit}$. We find that the 1990–1993 coeval hard and soft X-ray observations support the ADAF predictions. We discuss a new way to constrain black hole mass with spectral data and the ADAF theory and apply this technique to GRS 1758−258 to find $M_1 \gtrsim 8$–$9\ M_\odot$ at an assumed distance of 8.5 kpc. Further investigations of the ADAF model allow us to evaluate the model critically against the 1996 data and flux-flux diagram of Barret, McClintock, & Grindlay and to understand the limits of the latter's "X-ray burster box."

Subject headings: accretion, accretion disks — black hole physics — gamma rays: observations — radio continuum: stars — stars: individual (GRS 1758−258) — X-rays: stars

1. INTRODUCTION

GRS 1758−258 is one of the most fascinating objects in the X-ray/gamma-ray sky, and we have much to learn about it yet. For being second only to 1E 1740.7−2942 as the brightest persistent gamma-ray source near the Galactic center (Main et al. 1999), GRS 1758−258 remains an enigma. Not only do its remoteness and high column density obscure it but its proximity to GX 5-1, which delayed its discovery until 1990, even now poses a minor obstacle to low-energy ($\lesssim$25 keV) observations.

The few established facts about GRS 1758−258 are tantalizing. The search for a counterpart in the optical and infrared turned up no distinct result but only two or more candidates within 1″ (Martí et al. 1998). Even more interestingly, Rodríguez and collaborators working with the Very Large Array (VLA) found not one but at least three radio sources near the X-ray source that have a roughly jetlike symmetry with respect to it (Rodríguez, Mirabel, & Martí 1992). This weak jet structure reveals GRS 1758−258, like its neighbor 1E 1740.7−2942, to be a microquasar (Mirabel et al. 1993; Mirabel et al. 1992b) but with a lower column density than 1E 1740.7−2942 (see, e.g., Main et al. 1999), making it more amenable to observation. GRS 1758−258 also shows similarities to Cygnus X-1 in that persistent, low-level hard emission dominates its luminosity (Tanaka & Lewin 1995; Liang 1998). This persistence puts GRS 1758−258 among the type III black hole binaries (BHBs) of Zhang et al. (1997b), while the radio jets put it among Zhang et al.'s type II BHBs.

In this paper we combine published and publicly available data from high-energy missions and the VLA to produce a long-term light curve for the source in the radio and in soft and hard X-rays. We performed our own reduction of the VLA data, including several observations without published results. In the first part of the paper (§ 2), we enumerate the diverse data sources that we have tapped and our handling of them, especially of the 1990–1993 *ROSAT* observations (§ 2.2), which are the only soft X-ray observations bridging the 1991–1992 hard X-ray dip.

Second, we compare the data from the various data sets with each other and with results of observations of other celestial objects (§ 3). Most notably, we find (§ 3.1) no ultrasoft component throughout the 12 years spanned by the soft X-ray observations, strongly arguing against the possibility that GRS 1758−258 was in the high state at any of those times. We investigate possible correlations of hard X-rays with soft X-rays and the hard X-rays with spectral shape.

In § 4 we combine the *ROSAT* data with those of *Granat* to constrain models of accretion disk emission: the advection-dominated accretion flow (ADAF) model (§ 4.1), the two-temperature model (§ 4.2), and the disk corona model (§ 4.3). Finally, in § 5 we show that the ADAF model explains properties of the flux-flux diagram and "X-ray burster box" of Barret, McClintock, & Grindlay (1996, hereafter BMG), and we evaluate the model in light of the diagram and data of that paper.

2. OBSERVATIONS

In Figure 1 we combine data from many instruments to produce a long-term light curve and spectral index history

[1] Columbia Astrophysics Laboratory, 538 West 120th Street, New York, NY 10027; jwk@phys.columbia.edu.
[2] Lawrence Livermore National Laboratory, 7000 East Avenue, Livermore, CA 94550.
[3] Space Radiation Laboratory, California Institute of Technology, MS 220-47, Pasadena, CA 91125.
[4] Department of Physics, University of California at Santa Barbara, Santa Barbara, CA 93106.
[5] Jet Propulsion Laboratory, California Institute of Technology, 4800 Oak Grove Drive, Pasadena, CA 91109.

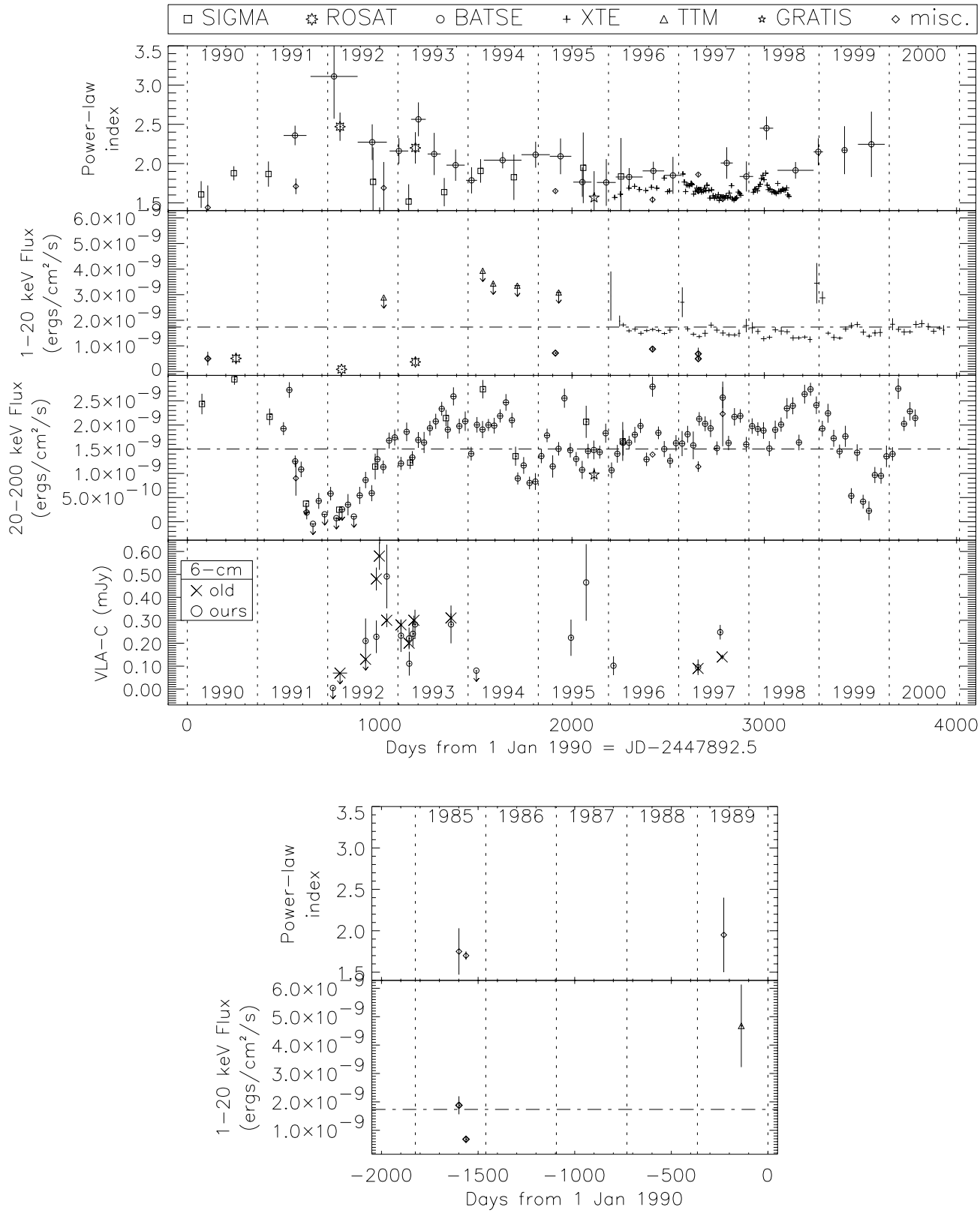

FIG. 1.—Light curve and spectral index history for GRS 1758−258 for 1985–2000. Provenance of miscellaneous data points is given in Table 2. Photoelectric absorption has been removed from the low-energy X-ray fluxes by assuming that the intrinsic spectrum is a power law that continues to lower energies. Power-law indices with errors greater than 0.4 have been omitted for clarity. The dash-dotted lines indicate the burster box boundaries of BMG for an assumed distance of 8.5 kpc.

TABLE 1

INSTRUMENTS NAMED IN FIGURE 1

Instrument	Band (keV)	Reference
Granat/SIGMA	30–1300	See text; see Kuznetsov et al. 1999
ROSAT/PSPC	0.1–2.5	This work
ROSAT/HRI	0.1–2.5	This work
CGRO/BATSE	20–1000	This work
RXTE/PCA (PLI).....	2–60	Main et al. 1999, Fig. 2
RXTE/ASM (flux).....	1.5–12	This work
Mir-Kvant/TTM	1–20	See text; see Aleksandrovich et al. 1998
GRATIS	20–200	This work

for the source. The soft X-ray light curve is of unabsorbed flux.

Below we briefly describe the major instruments and how the data were derived. Other instrument characteristics are listed in Table 1. Minor, miscellaneous instruments are listed in Table 2.

2.1. *Granat*

The ART-P and SIGMA telescopes on the Russian *Granat* satellite discovered GRS 1758−258 in 1990 March–April (Mandrou 1990). *Granat* observed the source seasonally through the spring of 1996.

The power-law indices in the plot come from Table 1 of Kuznetsov et al. (1999). This table contains results of fitting two seasonal spectra a year to a power law over the range 30–300 keV. Above 150 keV the spectrum decays exponentially. In order to get results comparable to other experiments' fits below 150 keV, we had to band-limit the *Granat* photon indices. We fitted the spectrum from the sum of their data (shown in their Fig. 5) below 150 keV in XSPEC to $\alpha = 1.825$. This index is 0.304 less than the power-law index for the full 30–300 keV range. We subtracted this number from each of their Table 1 indices to derive the band-limited index below 150 keV. This procedure assumes the temporal independence of the spectral shape, an assumption supported by the lack of evidence for change in spectral hardness (Kuznetsov et al. 1999).

The fluxes in the plot were produced by adding to the flux derived from their 40–200 keV luminosities (their Table 1), a power-law flux from 20–40 keV calculated using the just derived band-adjusted index.

2.2. *ROSAT*

ROSAT observed GRS 1758−258 in 1990 September, 1992 March, and the spring of 1993, spanning the hard X-ray dip of 1991–1992. In § 3 we use these data to constrain the corona models for disk emission and the ADAF model. They are pivotal to our argument that there was no ultrasoft component in 1993 and that the soft and hard X-rays tracked through the 1991–1992 dip.

Two groups have published analyses of the *ROSAT*/Position Sensitive Proportional Counter (PSPC) 1993 March 31–April 1 pointed observation of GRS 1758−258: Mereghetti, Belloni, & Goldwurm (1994) and Grebenev, Pavlinsky, & Sunyaev (1997). The original 1994 analysis found a high soft component and took source counts from a radius of 18′ around the source in an effort to collect dust-scattered photons; this analysis took background counts from five circles of radius 13′ in the external regions of the detector to avoid contamination by GX 5-1.

On the other hand, the 1997 reanalysis of the 1993 data showed a relatively low soft component and conjectured that the difference comes from "contamination of the field [of the original analysis] by the nearby very bright source GX 5-1." For this analysis, "source and background counts were extracted from a circle of radius 5′ and an annulus of radii 10′–15′ (both centered at the GRS 1758−258 position)" to exclude contamination by GX 5-1.

We conducted an independent analysis of the 1993 observation. In order to set the extraction radius for GRS 1758−258, we considered several factors. We wanted to include at least 90% of the photons from the source, taking into account the scattering halo (assumed to scale with that

TABLE 2

MISCELLANEOUS DATA POINTS IN FIGURE 1

Month/Year	Day[a]	Instrument	Band (keV)	Reference
1985 Aug	−1599	SL2/XRT	2.5–25	Skinner 1991
1985 Sep.....	−1562	*EXOSAT*/ME	1.5–50	This work
1989 May.....	−228	POKER	15–180	Bazzano et al. 1993
1990 Apr	106	*Granat*/ART-P	4–60	Sunyaev et al. 1991
1991 Jul.....	564	*CGRO*/OSSE	50–10^4	Jung et al. 1993
1992 Oct.....	1021	*Mir-Kvant*/HEXE	20–200	Maisack et al. 1993
1995 Mar.....	1914	*ASCA*/SIS	0.4–10	Mereghetti et al. 1997
1996 Aug	2419	*RXTE*/PCA-HEXTE	2.5–250	Heindl & Smith 1998
1997 Apr	2657	*BeppoSAX*/LECS	0.1–10	This work
1997 Apr	2657	*BeppoSAX*/MECS	1.3–10	This work
1997 Apr	2657	*BeppoSAX*/PDS	15–300	This work
1997 Aug	2784	HEXTE and OSSE	20–700	Lin et al. 2000b, HEASARC archive

[a] Referenced to 1990 January 1 = JD 2,447,892.5.

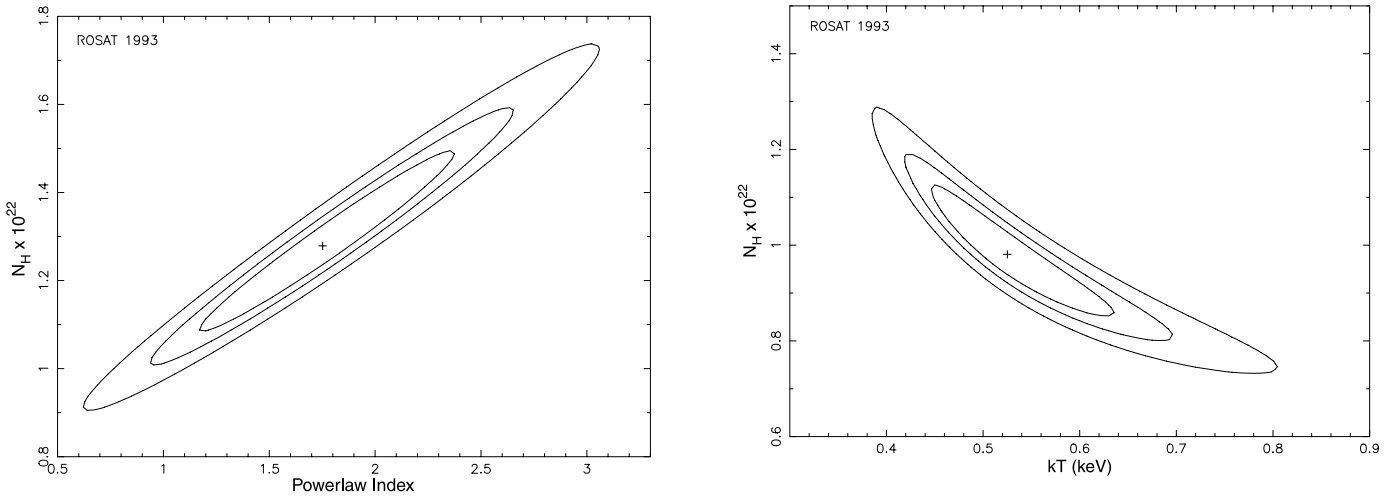

FIG. 2.—Confidence contours for fits to 1993 March data fitted to *ROSAT*/PSPC. *Left*: power-law fit. *Right*: blackbody fit

of GX 5-1; from Predehl & Schmitt 1995) while firmly excluding any photons from GX 5-1. In addition, we wanted to eliminate any contribution from the brighter background sources, in particular 1WGA J1800.2−2539 (localized only in 1995) at 13′.5 from GRS 1758−258. After examining several trial radii we compromised on an extraction radius of 9′, with background selected from a 9′ radius circle at the western edge of the detector. To exclude any possible contamination from GX 5-1, we extracted background from an area outside the central ring of the PSPC (see, e.g., Chu et al. 2000) rather than the usual annular region just outside the central source region.

After extraction, the data were fitted in XSPEC to a power law with photoelectric absorption and then to a blackbody with absorption, giving the respective best-fit values of $\alpha = 1.75 \pm 0.39$, $N_H = (1.28 \pm 0.13) \times 10^{22}$ cm^{-2} ($\chi^2_\nu = 0.879$, $\nu = 15$), and $kT = 0.53 \pm 0.06$, $N_H = (0.98 \pm 0.08) \times 10^{22}$ cm^{-2} ($\chi^2_\nu = 0.873$, $\nu = 15$). Figure 2 shows the error contours of our fits. It is noteworthy that the blackbody fit is inconsistent at more than the 4 σ level with the standard column ($\sim 1.5 \times 10^{22}$ cm^{-2}) for the source (Mereghetti et al. 1997; Heindl & Smith 1998; Main et al. 1999). We will more fully address the blackbody fit in § 3.1, but suffice it to say for now that our fits indicate that the blackbody component is incompatible with the accepted column for the source.

The count rate for the 7900 s 1993 spring observation was 1.32 ± 0.02 counts s^{-1} for 0.1–2.4 keV. The 1990 September 10–12 All-Sky Survey observation of the source had a slightly higher count rate of 1.81 ± 0.12 counts s^{-1} for the same energy range. This count rate comes from the High Energy Astrophysics Science Archive Research Center (HEASARC) *ROSAT* All-Sky Survey Bright Source Catalog, as revised in 1996, which supersedes the 0.95 ± 0.04 counts s^{-1} reported in Mereghetti et al. (1994). The latter paper used preliminary data to conclude that: "Soft and hard spectral components are anticorrelated [if one ignores the 1992 observation]. Between 1990 September and 1993 March both varied by about a factor of 2, but in opposite directions." Based on the more definitive count rate, we find no anticorrelation but rather a correlation between the 1990 and 1993 soft X-ray fluxes. The HRI observation from 1992 March 13 reported a rate of 0.15 ± 0.01 counts s^{-1}, statistically consistent with the 0.18 ± 0.01 counts s^{-1} reported in Mereghetti et al. (1994).

No spectral information is available from the 1990 *ROSAT* All-Sky Survey observation. The HRI data provide no spectral information. Thus, we have assumed the 1993 spectral shape for all three observations in deriving the unabsorbed fluxes in Table 3, which is quite reasonable given the large error bars on our photon index, which easily encompasses the majority of indices in Figure 1.

Grebenev et al. (1997) found for the 4100 s 1992 March 5 off-axis PSPC observation of GRS 1758−258 a power-law index of 2.47 ± 0.18. In contrast, we consider their flux for this observation to be somewhat suspect since the proper extraction area is not unambiguous in this distorted region of the focal plane.

TABLE 3

UNABSORBED 1.0–2.4 keV FLUXES FROM *ROSAT*

Observation Date	Original[a] ($\times 10^{-10}$ ergs cm^{-2} s^{-1})	Reanalysis ($\times 10^{-10}$ ergs cm^{-2} s^{-1})	Instrument
1990 Sep 10–12.....	1.4	1.12 ± 0.14	PSPC (survey)
1992 Mar 13.....	0.76	0.51 ± 0.06	HRI
1993 Mar 31–Apr 2.....	2.8	$0.82^{+0.11}_{-0.08}$	PSPC

[a] From Mereghetti et al. 1994.

In extrapolating *ROSAT* fluxes for Figure 1, we assume that the photon index of 1993 held for 1990, but we use Grebenev's value of 2.47 for the 1992 observation.

2.3. *Compton Gamma Ray Observatory*

The *Compton Gamma Ray Observatory* (*CGRO*)/BATSE data come from NASA's Marshall Space Flight Center; the 20–100 keV fluxes and their associated errors were produced by fitting each day's BATSE Earth occultation data to a power law with a spectral index of 1.8. To extend the energy range of the flux to 200 keV, we ignored the exponential cutoff above ~150 keV and simply continued the power-law index of 1.8 out to 200 keV (we added a 30% correction to better agree with the *Granat* fluxes).

Deriving the photon indices proved more of a challenge. For each viewing period, we produced the ".pha" and ".rmf" files with the standard FTOOLS "bod2pha" and "bod2rmf." We then fitted the data from each viewing period to a power law within XSPEC and recorded the results. To give the values plotted in the figure, we performed weighted averages of the spectral indices for each of three periods within each observational cycle. The errors on the indices are large, but they hint at a trend resembling an upside down cycloid, with a cusp occurring during the hard X-ray dearth of 1991–1992 and another in the dearth of 1999.

2.4. *Rossi X-Ray Timing Explorer*

The All-Sky Monitor (ASM) fluxes presented in Figure 1 are derived from "quick-look" results provided by the *Rossi X-Ray Timing Explorer* (*RXTE*)/ASM team and archived at MIT. These light curves are binned into three energy bands, 1.5–3, 3–5, and 5–12 keV. We converted these to fluxes by comparing the count rates with the average ASM crab count rates in each channel and extrapolated to 20 keV using a power-law index from the last two bands. The power-law indices ranged from ~1.7 to 2 but have been omitted from the power-law index plot because of their large errors (~0.8).

Except for the 2 month spike at the end of 1998 and the beginning of 1999, the ASM data is flat not only in Figure 1 but also in the individual bands. There is no sign of the oscillation from late 1999 February to September noted by Smith, Heindl, & Swank (1999). It is difficult to tell if the flatness is meaningful or the result of the inclusion of the Galactic diffuse emission or other discrete sources in the ASM's large field of view. It might be possible to subtract the diffuse emission, but, unfortunately, the sky coordinates and position angle of each pointing are not readily available.

2.5. *Other X-Ray Data*

Data from the 1997 April 10 *BeppoSAX* observation were obtained from NASA's HEASARC archive and fitted in XSPEC to a power law with (MECS) $N_{\rm H} = (1.68 \pm 0.05) \times 10^{22}$ cm^{-2}, $\alpha = 1.65 \pm 0.02$, $\chi^2_\nu = 1.17$ for $\nu = 95$ and (LECS) $N_{\rm H} = (1.64 \pm 0.05) \times 10^{22}$ cm^{-2}, $\alpha = 1.54 \pm 0.02$, $\chi^2_\nu = 1.13$ for $\nu = 107$. For the PDS data, we found $\alpha = 1.86 \pm 0.02$ with $\chi^2_\nu = 2.19$ for $\nu = 14$.

The *Gamma-Ray Arcminute Telescope Imaging System* (*GRATIS*) is a balloon-borne coded aperture imaging experiment consisting of 36 coaligned one-dimensional telescopes with a total effective area of 378 cm^2 at 30 keV. Each telescope consists of a 2 mm thick CsI(Na) crystal coupled to a photomultiplier tube passively collimated to have a field of view of 40′ × 3° (FWZI). The average energy resolution of the detectors is 19% at 60 keV. *GRATIS* is more fully described in Harrison et al. (1989) and Keck (2001).

GRATIS observed GRS 1758−258 from 5:43 to 6:43 hr UT on 1995 October 17. *GRATIS* was launched on its balloon from Alice Springs in the center of the Australian outback at 23.°80 south, 133.°40 east. To remove the background contribution, we subtracted the blank-field pointing that immediately preceded this observation (4:43–5:43 UT) centered at $\alpha = 17^{\rm h}23^{\rm m}57^{\rm s}$, $\delta = -37°50'39''$, epoch 2000. This field contains no known high-energy sources. GRS 1758−258 is at $l = 4.°51$, $b = -1.°36$, whereas the background pointing is at $l = -9.°93$, $b = -1.°03$. The two fields have a comparable contribution from the Galactic diffuse emission since the longitudinal variation is slow for $l < 10°$ (Iwan et al. 1982) and the latitudinal variation is nearly flat when $|b| \geq 1°$ (Valinia & Marshall 1998; Fig. 2*b*). GX 5-1 lay just on the edge of the fine-collimator field of view for the source pointing. In principle the rotations of some of the tubes should permit photons from GX 5-1 to fall into the coarse collimators' ~3° field of view. Omitting data counts from these tubes did not significantly alter the 20–132 keV fit.

We unfolded the source counts using the standard XSPEC package from NASA's HEASARC. The response matrix was constructed with the Lawrence Livermore National Laboratory's COG Monte Carlo photon transport package (Buck & Lent 1993; Wilcox & Lent 1989). A more detailed description of the data analysis can be found in § 4.1 of Keck (2001).[6] The best-fit power-law model to the data has a photon index of 1.57 ± 0.34 with a reduced χ^2 of 1.08 for 90 degrees of freedom. The flux was $(9.3 \pm 1.4) \times 10^{-10}$ ergs cm^{-2} s^{-1}.

The 1985 September *EXOSAT*/medium-energy experiment (ME) data came from the HEASARC archive data for EXO 1757−259, with GRS 1758−258 being 9.′4 off-center. The unfolded spectrum is plotted in Skinner (1991). The data file does not list the region of the detector from which the source counts were extracted, but the 45′ field of view (FWHM) of the ME means that the observation may include contamination from GX 5-1 in addition to the Galactic diffuse emission. Using XSPEC, we fitted the data to a power law with absorption $N_{\rm H} = (1.79 \pm 0.16) \times 10^{22}$ cm^{-2}, $\alpha = 1.70 \pm 0.05$, $\chi^2_\nu = 0.95$ for $\nu = 61$.

The 1–20 keV flux point and upper limits for *Mir-Kvant*/TTM have been extrapolated assuming a power-law index of 1.8. Our data are taken from the one detection and five upper limits of Aleksandrovich et al. (1998).

For completeness, we mention the flux of $(0.862 \pm 3.36) \times 10^{-10}$ ergs cm^{-2} s^{-1} and the power-law index of 1.95 ± 0.45 from the 15–180 keV POKER instrument (Bazzano et al. 1993). The error bar is far too large to add anything to the plot.

2.6. *Radio Data*

Radio fluxes measured by the VLA were originally published in Mirabel et al. (1992a), Mirabel & Rodríguez

[6] Available online at http://www.astro.columbia.edu/~jwk/thesis.pdf.

(1993), Rodríguez et al. (1992), and Lin et al. (2000b).[7] The 1997 April data point was provided by J. Martí (2000, private communication).

As part of our review of the data on GRS 1758−258, we performed our own reduction of the VLA observations of GRS 1758−258, including those in 1994, 1995, and 1996, which have not been previously published. Only in 1997 did the VLA begin observations of GRS 1758−258 at $\lambda = 3.7$ cm, when Lin et al. (2000b) noted a flat spectral index. We used the classic 1999 October 15 version of AIPS in our reduction. For all observations, the gain calibrator was 1328+307 (aka 3C 286, 1331+305), and the phase calibrator was 1748−253 (1751−253), except for the 1997 August 3 observation, which used 0134+329 (3C 48, 0137+331) for the gain calibrator. The phase calibrator had a boot-strapped flux density in the range 0.47–0.52 Jy. The upper limits in the plot of these points are 1 σ, while those for the previously published data are 4 σ.

The reanalyzed points are statistically compatible with the previously published results, as can be seen in the bottom panel of Figure 1. The four additional points our analysis adds to the light curve add no further correlation to the X-ray data.

3. RESULTS

We now further analyze and integrate the observations to compose a picture of GRS 1758−258.

3.1. *Blackbody Temperatures*

Mereghetti et al. (1994) claimed to find a soft X-ray excess in the 1993 data. Lin et al. (2000b) found that a fit to the 1997 multi-instrument observation with a power law with exponential cutoff was just as good without the blackbody ($\chi^2_\nu = 1.0$, $\nu = 620$) as with ($\chi^2_\nu = 0.92$, $\nu = 619$). Mereghetti et al. (1997) found that the fits to the *ASCA* data did not require a blackbody component since the model of a lone power law gave an acceptable ($\chi^2_\nu = 1.031$, $\nu = 872$) fit.

Unlike the 1994 paper, but in agreement with the latter two papers, we find that a blackbody component is not needed in the *ROSAT* data and in the observations of other soft X-ray missions.

As we mentioned in § 2.2, the typically observed column density for GRS 1758−258 of $\sim 1.5 \times 10^{22}$ cm^{-2} (Mereghetti et al. 1997; Heindl & Smith 1998; Lin et al. 2000b) lies far outside the 3 σ contour for our blackbody fit to the 1993 *ROSAT*/PSPC data, shown in Figure 2. Our best-fit column with this model [$N_{\rm H} = (0.98 \pm 0.08) \times 10^{22}$ cm^{-2}] is inconsistent with the usual column at the 4 or 5 σ level. (While this could be an anomaly resulting from a sudden absence of intrinsic absorption, we find this explanation unlikely in explaining one highly deviant result.) Additionally, the power-law model provides a good fit consistent with the standard column ($\chi^2_\nu \approx 0.97$; see Fig. 2).

We also fitted the data of other soft X-ray missions over 12 years. The spectra from all of these observations are very similar to the *ASCA* spectrum in Figure 3 of Mereghetti et al. (1997). Table 4 shows the values of χ^2_ν that result with and without a blackbody component added to the power law fit. The respective results are comparable, indicating that the ultrasoft component is unnecessary. As discussed above, the blackbody component is characteristic of the high state, so the lack of it indicates that none of these observations occurred in that state. Furthermore, the absence of any major hard X-ray flux changes strongly argues against the source changing states in this period. Thus, we conclude that the source was not in the high state in this period.

Mereghetti et al. (1997) estimated that to hide an ultrasoft component behind a hot corona requires a relatively large scattering opacity $\tau \sim 2$–5.

As expected, the blackbody temperatures fall in the range $\sim$0.2–1.0 keV. For comparison, the blackbody plus power law fit to the 1995 *ASCA* data in Mereghetti et al. (1997) found a blackbody temperature around 0.4–0.5 keV. The best-fit HT model of Lin et al. (2000b) to the 1997 August *RXTE* data gave a blackbody temperature of $T_{\rm BB} \approx 1.18$ keV .

3.2. *High- and Low-Energy Fluxes and the Flux-Flux Diagram*

Whereas an anticorrelation between the hard and soft X-ray fluxes is the usual sign of the transition between a low (hard) state and a high (soft) state, the correlation of the *ROSAT* data with the *Granat* data through the 1991–1992 dip indicates that such a transition did not take place.

Figure 3 illustrates the correlations, or lack of, between the hard X-ray (20–200 keV) luminosity and the soft X-ray (1–20 keV) luminosity in the manner of BMG.

The *RXTE*/ASM data does not show any significant correlation, positive or negative, to the hard X-ray dip in

[7] The 1992 July 16 flux quoted in Mirabel & Rodríguez (1993) supersedes that in Rodríguez et al. (1992) according to L. Rodríguez & J. Martí (2000, private communication).

TABLE 4

BLACKBODY MODEL TEMPERATURES

Date	Blackbody Temperature	Blackbody Normalization	Model[a]	χ^2_ν	χ^2_ν without Blackbody	Instrument	Notes
1985 Sep ...	0.2370 ± 0.6229	6.0×10^{-4}	BB+PL	1.095 (32)	1.037 (34)	*EXOSAT*/ME	$\alpha = 1.70 \pm 0.10$
1985 Sep ...	1.063 ± 0.1112	9.8×10^{-4}	BB+PL	1.048 (32)	1.037 (34)	*EXOSAT*/ME	$\alpha = 1.32 \pm 0.41$
1985 Sep ...	0.2603 ± 0.09307	1.7×10^{-3}	BB+CompST	0.993 (57)	0.985 (38)	*EXOSAT*/ME	
1993 Mar...	0.5734 ± 0.4028	1.0×10^{-3}	BB+PL	0.998 (13)	0.879 (15)	*ROSAT*/PSPC	
1993 Mar...	0.6488 ± 1.034	7.9×10^{-4}	BB+CompST	1.091 (12)	0.947 (14)	*ROSAT*/PSPC	
1995 Mar...	0.5374 ± 0.0265	7.1×10^{-4}	BB+PL	0.971 (280)	1.051 (282)	*ASCA*/SIS	
1995 Mar...	0.5292 ± 0.03627	5.8×10^{-4}	BB+CompST	0.974 (279)	1.029 (281)	*ASCA*/SIS	
1997 Apr ...	0.8710 ± 0.1429	3.0×10^{-4}	BB+PL	1.321 (78)	1.335 (80)	*BeppoSAX*/LECS	
1997 Apr ...	0.8744 ± 0.1281	3.1×10^{-4}	BB+CompST	1.341 (77)	1.357 (79)	*BeppoSAX*/LECS	

[a] "CompST" abbreviates the Sunyaev-Titarchuk Comptonization model, as implemented in XSPEC.

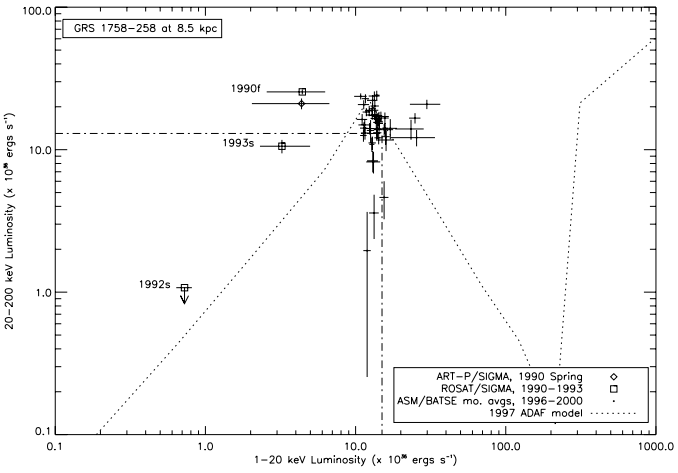

FIG. 3.—BMG style flux-flux diagram for GRS 1758−258 at an assumed distance of 8.5 kpc. The open plotting symbols represent points whose soft and hard coordinates are only approximately coeval. The ADAF model is scaled to $M_1 = 10.6\ M_\odot$ and is discussed in § 4.1. The dash-dotted lines indicate the burster box boundaries of BMG.

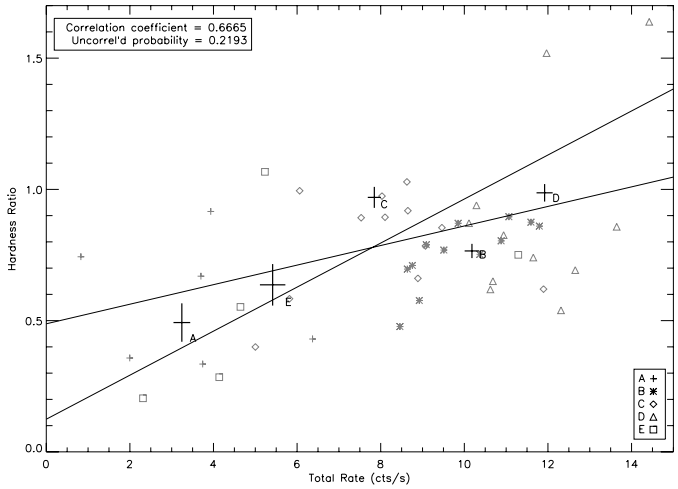

FIG. 4.—Hardness ratio vs. total count rate for 1990–2000 BATSE data. The crosses are averages binned with boundaries at 500 and 1000 (A), 1000 and 1700 (B), 1700 and 2600 (C), 2600 and 3400 (D), and 3400 and 3700 (E) days from 1990 January 1.

1999. Except for the 2 month spike at the end of 1998 and the beginning of 1999, the ASM data is flat, as shown in Figure 1 and in the individual bands. There is no sign of the oscillation from late 1999 February to September noted by Smith et al. (1999). It is difficult to tell if the flatness is meaningful or the result of the inclusion of the Galactic diffuse emission or other discrete sources in the ASM's large field of view.

3.3. *Correlation between Spectral Intensity and Shape*

Many black hole candidates (BHCs; see, e.g., Cyg X-1) display spectral pivoting so that the flux in a narrow energy band (∼10 keV) remains relatively constant in time, while the fluxes at higher and lower energies anticorrelate. This phenomenon occurs between the high and low states in what is known as the intermediate state. A consequence of spectral pivoting is that while the bolometric luminosity remains relatively constant (Zhang et al. 1997a), a correlation is established between the flux and power-law index in any given band above or below the pivot.

The *Granat* photon indices are consistent with a constant spectral slope because of the large error bars. We see a suggestion of a correlation between BATSE fluxes and spectral indices in Figure 1. For example, the flux dip of 1991–1992 has a higher index and therefore a softer spectrum.

We wanted to test for a correlation between the photon index and the flux, but calculation of flux assumes an index. Such a method can bias the results or exaggerate any correlation between intensity and shape.

The hardness ratio and count rate are good metrics for the photon index and flux and have the advantage of being independent of one another. It is difficult to compare raw count rates across instruments, so we restrict our analysis to BATSE data, which have the longest temporal baseline.

We plot the hardness ratio (ratio of counts above and below 78 keV) against the total BATSE count rate in Figure 4. The boundary between high and low counts is chosen to give a hardness ratio ∼1 on average. The thick crosses represent averages over five periods that have a similar total count rate throughout. From the slopes of linear fits to the averaged data, we find a linear correlation coefficient $r = 0.67$ (see § 11.2 of Bevington & Robinson 1992). The probability of an uncorrelated parent distribution having a coefficient that is big or bigger is only ∼22%, so there is a weak correlation between shape and intensity. Consequently, we expect lower fluxes to have higher, softer photon indices, a conclusion that agrees with the predictions of the ADAF theory discussed in § 4.1.

4. DISCUSSION

Here we describe three models to account for the observed emission from GRS 1758−258. In all of these models, the soft X-ray emission comes from the disk and the hard X-ray emission comes from the corona or hot-electron cloud. The first is the advection-dominated accretion flow model, which we apply in a novel way. The latter two are standard Keplerian accretion models.

In our discussions of the latter two models, we assume the argument of Shapiro, Lightman, & Eardley (1976, hereafter SLE) that the seed photons range in energy from 0.05 to 5 keV. (The exact mechanism of emission is not important, but possibilities include blackbody emission from the disk and synchrotron radiation from disk electrons, as explained in SLE; Zhang et al. 1997b.) In these models, we explain the correlation between the hard and soft X-rays as a consequence of the Comptonization of soft X-rays into hard X-rays by the corona. The accurate determination of the *ROSAT* fluxes is critical here since we extrapolate the soft X-ray flux from that data.

4.1. *Advection-Dominated Accretion Flow*

We begin with the advection-dominated accretion flow model. This is the most mature model of blackhole accretion in that its proponents have published spectral predictions (Esin, McClintock, & Narayan 1997, hereafter EMN; Esin et al. 1998). Thus, we decided to test the model in detail for GRS 1758−258 and to scout out the theory-testing terrain that imminent observational improvements will open to detailed exploration.

The accretion flow has two zones: an inner advection-dominated flow and an outer thin accretion disk. The inner

ADAF accretes into the black hole as a quasi-spherical two-temperature corona, while the thin disk is Keplerian. The soft X-ray emission comes from the disk, and the hard X-ray emission comes from the corona.

The present model resembles the two-temperature model of SLE with the difference that the transition radius between the quasi-spherical and Keplerian zones r_{tr} changes with the accretion rate. The most notable characteristic of the model is that the state of black hole accretion, as illustrated in Figure 1 of EMN, is controlled by one parameter, the mass accretion rate $\dot{m} \equiv \dot{M}/\dot{M}_{Edd}$, where $\dot{M}_{Edd} \equiv L_{Edd}/0.10c^2$. The last definition assumes a 10% radiative conversion efficiency. (This assumption is restricted to this definition; the radiative efficiency ϵ of the model itself varies with $\dot{m}$.)

In other words,

$$\dot{m} = \left[\frac{L}{\epsilon(\dot{m})c^2}\right]\left(\frac{0.10c^2}{L_{Edd}}\right)$$

or

$$L \propto \dot{m}\epsilon(\dot{m})L_{Edd} .$$

Another significant feature of the ADAF theory is the scale invariance of the states: the theory is the same for black holes of any size, from Galactic to supermassive (Narayan & Yi 1995), which means that the radiative efficiency for a given $\dot{m}$ is independent of black hole (primary) mass, that is $\epsilon \neq \epsilon(M_1)$. Since the Eddington luminosity scales with the primary's mass, the luminosity of any given state also scales with mass, thus establishing a correlation between black hole mass and luminosity at known $\dot{m}$:

$$L = L(\dot{m}) \propto M_1 .$$

If we know $\dot{m}$, we can compare the model luminosity at a given mass to measured luminosity to find the mass of the observed black hole (M_1). Note that this proportionality of luminosity in a given state to black hole mass holds for any model whose radiative efficiency is similiarly independent of black hole mass.

We now use the mass-luminosity correlation and the observed flux extremes to constrain the mass of GRS 1758−258. Since the ADAF models scale with primary mass, the scale factor that best allows the model to fit the data fluxes is the same factor that must multiply the model's assumed mass. In theory, the model's mass scaled by the factor is then the mass of the primary. In reality, other model parameters such as the binary's inclination angle i, viscosity α, and the fraction of the total pressure due to gas (as opposed to magnetic) pressure β also affect the luminosity, although they do not affect all energies and all states uniformly, as does the primary mass M_1. Additionally, since the model predicts *luminosities*, while we measure *fluxes*, our technique only gives us the primary mass at an assumed distance d_0; so instead of M_1, we find $M_1/(d/d_0)^2$.

We take the ADAF model from the νL_ν curves of EMN for $M = 6\ M_\odot$, $i = 60°$, $\alpha = 0.25$, $\beta = 0.5$ for Nova Muscae and of Figure 1*b* Esin et al. (1998) for $M = 9\ M_\odot$, $i = 40°$, $\alpha = 0.3$, $\beta = 0.5$ for Cyg X-1. The luminosities of the high-state spectra for the 1997 model are not exactly correct because the high-state curves in Figure 10 of EMN do not extend out to 200 keV. To overcome this limitation, we have replaced the $\dot{m} = 0.40$ curve with its suitably renormalized counterpart from Figure 1*a* of Esin et al. (1998); the two curves agree to a constant factor for their common energies. The remaining high-state hard luminosities are integrated from linear extrapolations, which may make them slightly high, although not by much, judging from the extrapolation of the $\dot{m} = 0.4$ curve.

The 1998 model is an incremental improvement to the 1997 model. Observational evidence from Życki, Done, & Smith (1997) that the transition radius varies in the low state and not exclusively in the intermediate state moved the model's authors to incorporate this feature. Other changes reflect that a different source is being modeled. Figure 4*a* of EMN makes it clear that $i = 30°$ instead of $i = 60°$ increases the flux ~25% in both soft and hard X-ray bands, at least for the low state. The change in α is more complicated since its value affects the value of $\dot{m}_{crit}$. For $\alpha = 0.25$, $\dot{m}_{crit} \approx 0.082$, while for $\alpha = 0.3$, $\dot{m}_{crit} \approx 0.11$, and the flux shifts to harder energies at the critical value according to EMN's Figure 4*b*. The 1998 theory models Cyg X-1, but the authors do not make clear how its wind-driven nature affects the model.

We find that the minimum scaling factor for the model fluxes to produce the maximum observed hard X-ray fluxes is 1.43. For consistency, we can check that the *Granat* and *ROSAT* minima from the 1991–1992 dip are still possible with this multiplicative factor; we can also check the coeval photon indices. Figure 5 shows the model integrated over hard and soft energy bands as thick curves, along with the observed flux extremes in those bands, plotted as thin horizontal lines with hatched error bands. The ordinate is $p\dot{m} \equiv -\log \dot{m}$, so higher $\dot{m}$ is to the left. We begin in the low state on the right-hand side. Moving from right to left as $\dot{m}$ increases, we see both the hard (*dashed curve*) and soft (*solid curve*) fluxes increase monotonically until we cross the first dotted vertical line, past which $p\dot{m} > p\dot{m}_{crit}$, putting the flow into the intermediate state. The transition radius r_{tr} rapidly contracts as we move to the left, and the hard and soft emission bands "swap" intensities. As we further increase $\dot{m}$ past the second dotted line, the flow enters the high state, in which the soft flux increases while the hard flux decreases. The second panel of Figure 5 shows the power-law indices predicted by the model and observed by *Granat* and *ROSAT*. Note that the model's hard X-ray power-law index increases with decreasing flux, in agreement with the intensity-shape correlation we saw in the BATSE data (§ 3.3).

We find that the theory is consistent with the *Granat* and *ROSAT* observations. The scaling factor multiplying the maximum hard model flux is just enough to reproduce the maximum *Granat* flux in 1990 of 92.5 ± 3.8 mcrab at the 3 σ lower limit. The factor also allows the soft model flux to match the 1992 *ROSAT* observed flux minimum at the same $p\dot{m}$ since the hard model flux falls below the coeval *Granat* upper limit. In the lower panel we see that the model's hard photon index just brushes against the top error bar of the *Granat* 1990 index at approximately the same $p\dot{m}$ at which the 1990 *Granat* maximum occurs. At the $p\dot{m}$ of the 1992 flux minima, the model's soft photon index is well within the error bar of what we assume to be the coeval *ROSAT* index. So we find that the ADAF theory can consistently reproduce the *Granat* flux maximum and the *ROSAT* minimum at the same time as it predicts a hard X-ray flux that falls below the *Granat* upper limit.

Furthermore, if we attribute the multiplicative factor of 1.43 to primary mass alone, then to agree with the *Granat*

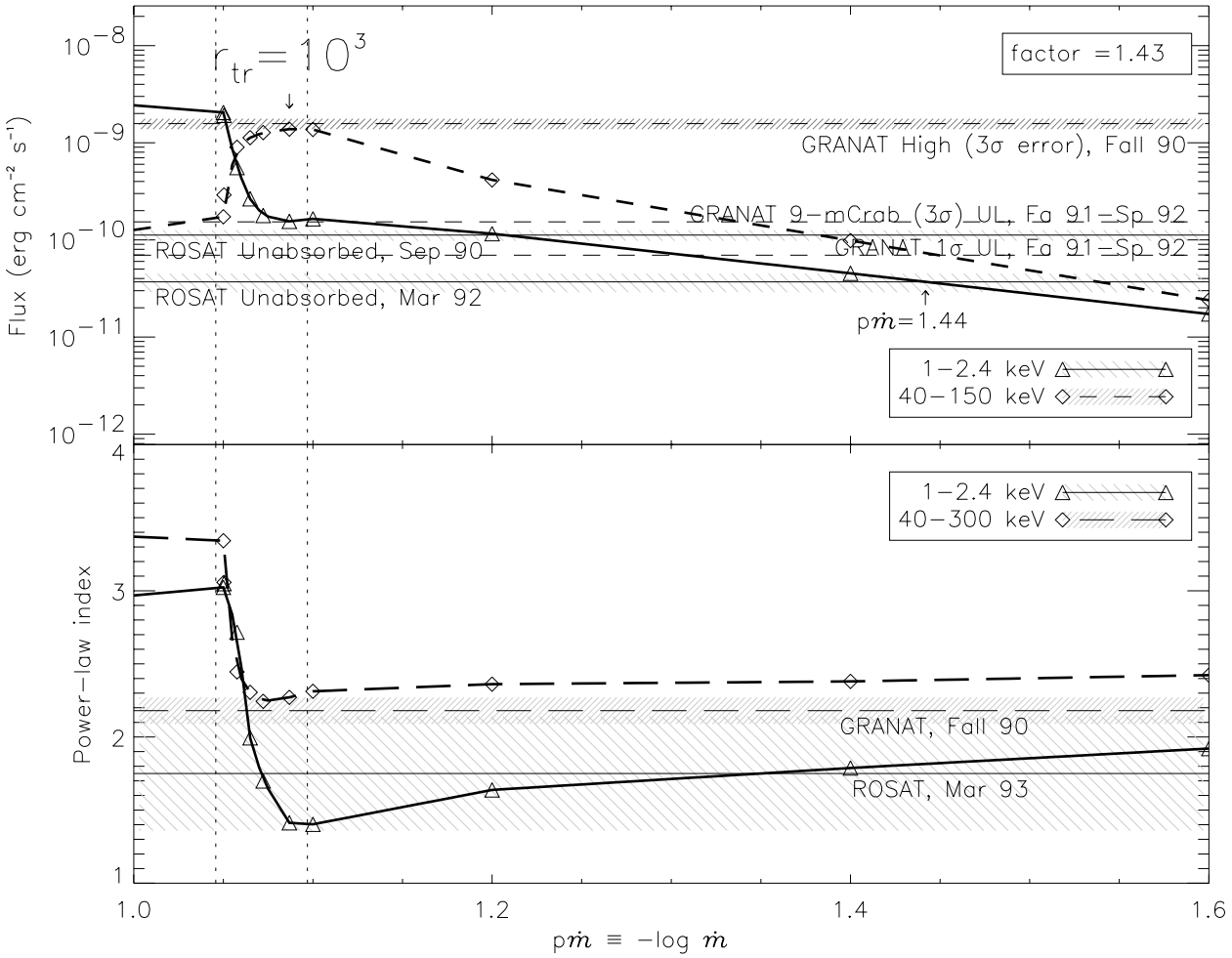

FIG. 5.—Results of the simple calculation of the multiplicative factor for the 1997 model. The 1990 and 1997 *Granat* fluxes are taken from Fig. 1 of Kuznetsov et al. (1999) and the power-law indices from their Table 1. The 1 σ 1992 *Granat* upper limit is calculated from data of Table 2 of Gilfanov et al. (1993).

1990 fall high at the 3 σ level, we must have $M_1/(d/8.5\ \mathrm{kpc})^2 \gtrsim 8.6\ M_\odot$.[8] Again, we note that the spectral consequences of the assumed values for inclination angle, viscosity, and fractional gas pressure are not clear from the published ADAF papers.

We could achieve a more sophisticated constraint on the factor by running all of the *ROSAT* and *Granat* flux and photon index data through a χ-squared analysis, but the authors of the theory warn that "the uncertainties in the model are still too large to draw meaningful quantitative conclusions" (Esin et al. 1998), so such an analysis is unwarranted with the theory as it now stands.

This mass is similar to that found for Cyg X-1, which is interesting because Cyg X-1 similarly remains in the low state usually with only occasional forays into the high. Unlike Cyg X-1, which has a massive companion and accretes via wind, the nondetection of an optical companion for GRS 1758−258 constrains its mass to $\lesssim 4\ M_\odot$ (Chen, Gehrels, & Leventhal 1994), so it must accrete by Roche lobe overflow. The other dynamically confirmed BHBs with identifiable secondaries also accrete by Roche lobe overflow, but most of them have also been seen in a very high state (see Fig. 6, discussed in § 5).

[8] The 1998 paper samples spectra more sparsely in $p\dot{m}$, so it is not clear what would be gained by a similar analysis with it.

4.2. *Comptonizing Donut Model*

While our primary goal was to study the ADAF model, we thought it worthwhile to use our data with the two-temperature and corona models to derive analytic estimates for some relevant parameters.

We apply the data to the two-temperature model of SLE. The best fits to the 1993 spring observations data from *ROSAT* and *Granat* give $\alpha_{\mathrm{soft}} = 1.8 \pm 0.4$ and $\alpha_{\mathrm{hard}} \approx 1.5 \pm 0.2$. We use these indices to extrapolate the hard and soft fluxes measured by these missions to the required energy bands: $F_{\mathrm{soft,\,obs}}(0.05\text{–}5\ \mathrm{keV}) = (3.4 \pm 1.6) \times 10^{-10}$ ergs cm^{-2} s^{-1} and $F_{\mathrm{hard}}(5\text{–}150\ \mathrm{keV}) = (1.30 \pm 0.19) \times 10^{-9}$ ergs cm^{-2} s^{-1}. So $L_{\mathrm{soft,\,obs}}/L_{\mathrm{hard}} = 0.26 \pm 0.13$.

We use these fluxes to derive model parameters. Combining the model's assumed cloud temperature of $\sim$50 keV with α_{hard}, we obtain $\tau \approx 2.0$. Our result agrees with others. Kuznetsov et al. (1999) fitted the 1990–1997 *Granat* data to a Comptonized disk model and found $\tau \approx 1.2$ and $T \approx 41$ keV. On the other hand, the best-fit HT (Titarchuk 1994; Hua & Titarchuk 1995) plus blackbody model of Lin et al. (2000b) to the 1997 August *RXTE* data gave $\tau \approx 3.4$ with an electron (cloud) temperature of $T \approx 52$ keV.

We likewise find from our data the scattering fraction $\zeta \approx 20\% \pm 12\%$. So less than one-third of the soft X-rays need be upscattered by a Comptonizing cloud that pushes the bounds of optical thinness to give the hard X-ray ($\gtrsim 5$ keV) spectrum in the spring of 1993. This result is consistent with the $\sim 10\%$ SLE found by applying their model to Cyg X-1. Our simple analytic results agree with the broad conclusions of others concerning general model parameters.

4.3. *Partial Disk Corona*

We now consider the disk corona model first proposed by Liang & Price (1977) and Bisnovatyi-Kogan & Blinnikov (1977) as an alternative to the two-temperature model that would stabilize the disk. In this model the corona is adjacent to the disk and sandwiches it from above and below like an undersized hamburger bun. See Liang (1998) for further discussion.

As with the previous model, the disk emits soft X-rays $L_{\rm soft}$, which are then Compton up-scattered to produce the hard X-rays $L_{\rm hard}$. The corona covers some fraction ξ of the disk, so $(1 - \xi)$ of the original photons have no chance of interacting with it. If the corona's optical depth is τ, another $\xi e^{-\tau}$ of the original photons pass through the corona unaffected. The formalism for deriving the covering fraction in terms of observables is identical to that of the previous model, with $\zeta = \xi(1 - e^{-\tau})$. The covering fraction is then

$$\xi = \frac{1}{1 - e^{-\tau}} \left(1 + \frac{A L_{\rm soft,\,obs}}{L_{\rm hard}} \right)^{-1} .$$

The extrapolated luminosity ratio (150:5.0:0.05 keV) from the 1993 spring *ROSAT* and *Granat* data remains $L_{\rm soft,\,obs}/L_{\rm hard} = 0.26 \pm 0.13$. From the *Granat* 1993 spring Comptonized disk model temperature of ≈ 85 keV and $\alpha_{\rm hard} = 1.5 \pm 0.2$, we find $y \approx 1.6$ and $\tau \approx 2.4$. For this y, we get the same amplification factor as for the previous model, $A \approx 15 \pm 5$, so the covering fraction $\xi \approx \zeta / [1 - \exp(-\tau)] = 9\%$–$35\%$. So less than about one-third of the emitting region of the disk was covered by a corona in the spring of 1993.

Our purely spectral analysis provides independent confirmation of results from timing data. Lin et al. (2000a) found that the lack of PDS steepening with increasing photon energy eliminated the $\zeta \sim 1$ model investigated by Böttcher & Liang (1998). T. J. Maccarone & P. S. Coppi (2001 private communication) found a $\sim 25\%$ reprossessing fraction by interpreting the soft X-ray lags in XTE J1748−2848 with a radiative feedback model.

5. FURTHER INQUIRIES WITH THE ADAF MODEL

We now explore the ADAF model in the context of the flux-flux diagram of BMG. We find that the ADAF model explains the boundaries of the "burster box" and reveals a gap in the diagram's differentiation of black holes from neutron stars.

In Figure 6 we re-present Figure 13 of Barret et al. (2000) overlaid with the tracks of the ADAF models of EMN and Esin et al. (1998). To make the comparison meaningful, we have scaled the luminosities of each BHB by $3\,M_\odot/M_1$ and the 1997 and 1998 models by $3\,M_\odot/6\,M_\odot$ and $3\,M_\odot/9\,M_\odot$, respectively. So assuming that the scale invariance of the ADAF model holds, we normalize the luminosities to $M_1 = 3\,M_\odot$.

With one exception, all of the BHBs are in reasonable agreement with the theory (although, since BMG's data lack error bars, it is difficult to tell what reasonable means). The solid points show the BHBs at their highest observed hard luminosities, so it is no surprise that the plot catches them either at the corner that represents $\dot{m}_{\rm crit}$ or in the very high state. The 1996 paper flags A0620−00 as having a somewhat doubtful hard X-ray tail. With that one exception, the models appear to have good agreement with the theory, including the very high state theory. No one value for the fraction of disk energy dissipated directly in the corona η clearly stands out, but $\eta = 0.5$ is reasonably close

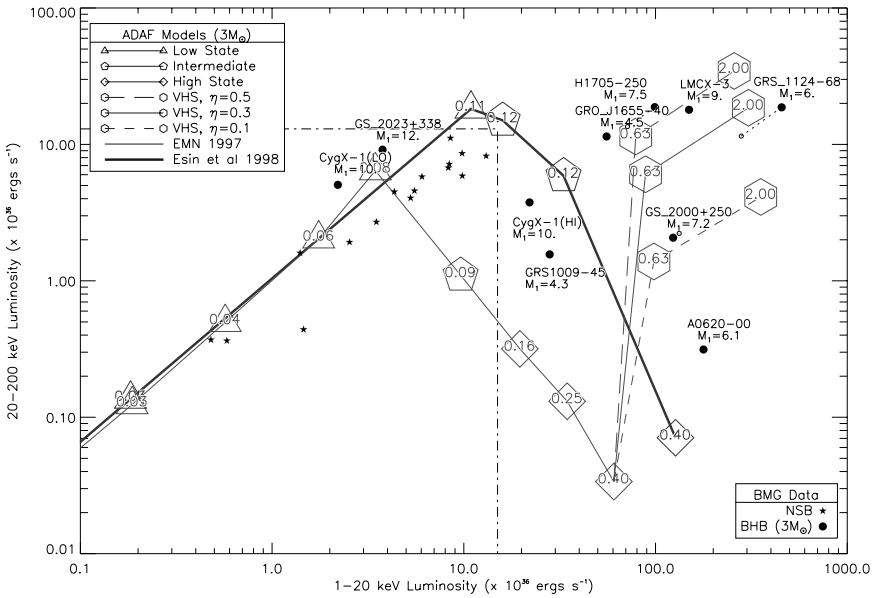

FIG. 6.—Plot of Barret et al. (2000; see BMG). The neutron star luminosities are unabridged, but the black hole luminosities have all been renormalized to $3\,M_\odot$. Overplotted for comparison is the ADAF model of EMN and Esin et al. (1998), and normalized to that same mass. Small open circles are based on the second distance estimate in BMG. The numbers in the polygons are the model values of $\dot{m}$ at each point. The dash-dotted lines indicate the burster box boundaries of BMG.

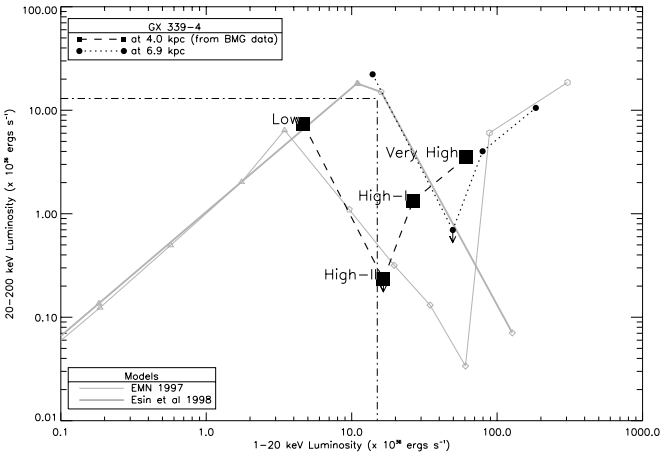

FIG. 7.—Data from Fig. 3 of BMG. Overplotted for comparison are the ADAF models of EMN and Esin et al. (1998) renormalized to $M_1 = 3\,M_\odot$. The state names are those of BMG and are somewhat different than in the ADAF model.

to three BHB points, whereas the other two values of η have only one each. It is remarkable that the 1998 theory, which was constructed for Cyg X-1, predicts soft X-rays that are not only overluminous in both low and high states but that are both overluminous by the same factor of ~ 1.8. A similar factor is obtained for GRS 1009−45, whose mass has only recently been measured (Filippenko et al. 1999).

Remarkably, the 1998 theory places the transition between low and intermediate states, which is the first simultaneous maxima of soft and hard X-rays, at the corner of the burster box. Notice that the neutron star binaries (NSBs), which have not been renormalized by mass, lie along the theory's low-state line (which runs roughly parallel to the $y = x$ line along which the luminosity points scale with Md^2). Consequently, the BMG plot does not distinguish *low-state* BHBs from NSBs. Since NSBs would likely show a blackbody component (Narayan, Garcia, & McClintock 1997) and this component appears in BHBs only with the onset of the intermediate and high states, perhaps the presence or absence of the blackbody component would distinguish NSBs from BHBs within the box.

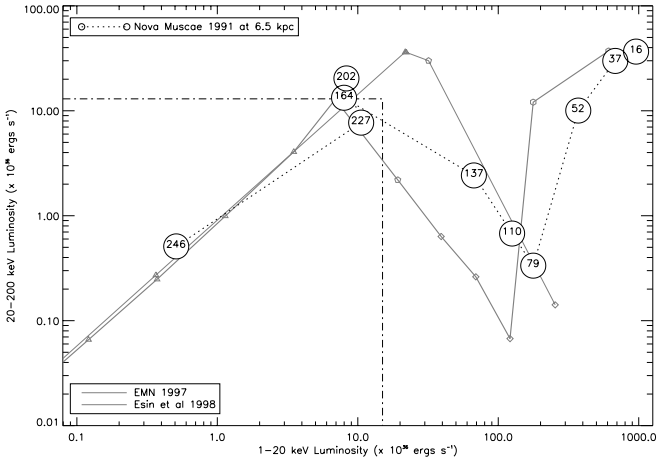

FIG. 8.—Data from Fig. 2 of BMG. Underlaid for comparison are the ADAF models of EMN and Esin et al. (1998) renormalized to the mass of Nove Muscae, 6 $M_\odot$. The numbers enclosed in the circles represent the day of the year 1991 for each point; the dotted line is only to guide the eye.

This criterion falls short if the 1997 model is the more accurate because the model predicts that intermediate-state and some high-state black holes fall in the box.

BMG's Figure 3 shows the plot for four observations of GX 339−4 at an assumed distance of 4.0 kpc. The points in the plot are labeled from left to right as "Low state," "High state II," "High state I," and "Very high state" (the nomenclature is apparently different from that of the ADAF papers). In Figure 7 we compare this data to the ADAF models at minimal (3 $M_\odot$) black hole mass. We see that the high-state segment of the 1997 $\alpha = 0.25$ model agrees reasonably well with the data but that the "high-I data point" (third from left) is somewhat distant from both the high and the very high state segments. EMN caution that their very high state is speculative. Esin et al. (1998) do not treat this state for Cyg X-1, so we do not know how the very high state theory changes with the change in parameters between the papers, but it is safe to assume that it cannot change without losing agreement with the BHB points on the BMG plot of Figure 6. This part of the theory comes reasonably close to the data as well as gives good agreement between the data and the 1998 $\alpha = 0.30$ model for the low and high states, on the assumption that GX 339−4 is a factor of $\sim\sqrt{3}$ more distant, in closer proximity to the Galactic center (~ 7 kpc). The typical absorption column to the source [(1–9) $\times\ 10^{21}$ cm^{-2}; Belloni et al. 1999; Méndez & van der Klis 1997] is consistent with this conclusion. Of course, any agreement with the ADAF theory presumes that the source is in fact a black hole, a premise that is not without dissent (see, e.g., Cowley, Crampton, & Hutchings 1987). The same authors estimate the 4.0 kpc distance to the source from its color and by assuming that its interstellar line velocity is due to differential rotational in the Galactic plane.

BMG's Figure 2 shows the plot for 10 points from the burst of Nova Muscae 1991 (GRS 1124−68) after its X-ray maximum on January 16 of that year. In Figure 8 we compare this data to the ADAF models at black hole mass (6 $M_\odot$). Recall that the model of EMN was constructed to fit this source. It is not surprising that the EMN model fails to fit the very high state data since the model's authors ventured only a tentative proposal for that state. What is surprising is that the high-state model is so far removed from the data since Figure 12 of EMN primed us to expect that the model was in much better agreement with this state.

6. CONCLUSION

We have seen that the preponderance of the data indicates that GRS 1758−258 was in a low state in the early 1990s since there was no blackbody component (§ 3.1) and that the soft and hard X-rays were correlated (§ 3.2; lack of dependable soft X-ray data prevents us from speaking about the 1999 X-ray dearth). We found a correlation between the hard X-ray spectral intensity and shape.

We applied the data to three models of accretion disk emission and used them to constrain the geometries of the Comptonizing torus (§ 4.2) and the disk corona models (§ 4.3). In the former, two-temperature model, less than one-third of the soft photons are upscattered to give the observed hard emission, while the latter disk corona model would say that about the same fraction of the disk is covered by a $\tau \approx 2$ corona, consistent with the $\sim 10\%$ reprocessing fraction found by SLE in applying their theory to Cyg X-1.

In § 4.1 we found that the coeval *Granat* and *ROSAT* data were consistent with the ADAF theory for an accreting black hole that spends most of its time in the low state but perhaps occasionally sidles up into the intermediate state. The correlation between the hard X-ray intensity and spectral shape observed in the BATSE data (§ 3.3) further supports the theory. We then introduced a new technique for constraining the mass of the primary and applied it to GRS 1758−258. With the present data, we constrained the mass of the black hole primary $M_1/(d/8.5\ \mathrm{kpc})^2 \gtrsim 8.6\ M_\odot$.

In § 5 we critically assessed the ADAF model against the flux-flux diagram of BMG. We found that the ADAF model explains the high-luminosity corner of the burster box but also raises the possibility that the box includes not only the advertised neutron stars but also some low-luminosity black holes. Furthermore, we found differences between the ADAF model and BMG's data for Nova Muscae 1991 and GX 339−4. The discrepancy for the latter appears to be overcome by positing a distance of ∼7 kpc instead of 4.0 kpc.

For a more critical test of the ADAF theory along this same line, additional data from binaries in various states are necessary. Continuous all-sky monitoring in both the soft and hard X-ray bands, such as would be provided by EXIST (Grindlay et al. 2000a, 2000b), would be key to this effort, and the luminosity's mass scaling allows us to compare directly the tracks of black holes of diverse masses across a flux-flux diagram such as BMG's. (Since many BHCs have exponential tails $\gtrsim$100 keV [Liang 1998], lowering the upper limit of the hard flux of the diagram to ∼100 keV could well improve its convenience and resolving power in comparing BHCs.) Timing signatures (see, e.g., Belloni et al. 1999) could then establish the corresponding accretion state.

This research was partially funded by NASA's Graduate Research Fellowship, NASA SRT, Lawrence Livermore (LLNL) IRD, and DOE NN-20. Work performed at the University of California Lawrence Livermore National Laboratory is supported by the US Department of Energy under contract W7405-ENG-48. It has made use of data obtained through the High Energy Astrophysics Science Archive Research Center Online Service, provided by the NASA/Goddard Space Flight Center, and extensively used NASA's Astrophysics Data System Abstract Service. We thank Michael McCollough and Colleen Wilson-Hodge of MSFC for graciously providing the *CGRO*/BATSE data and Josep Martí for the 1997 April VLA data point. The unseen but indispensable hands behind *GRATIS* include Dennis Carr, Chris Adams, Todd Decker, Jim Hughes, Greg Sprehn, Leigh Brookshaw, Craig Brooksby, Bob Priest, Matt Fischer, and Irwin Rochwarger. Thanks to David Helfand for his help negotiating the tortuous AIPS package and to the National Scientific Ballooning Facility for making the *GRATIS* flight possible. We thank the referee for the promptness of his comments.

REFERENCES

Aleksandrovich, N. L., Borozdin, K. N., Emel'Yanov, A. N., Sunyaev, R. A., & Skinner, G. K. 1998, Astron. Lett., 24, 742
Barret, D., McClintock, J. E., & Grindlay, J. E. 1996, ApJ, 473, 963 (BMG)
Barret, D., Olive, J. F., Boirin, L., Done, C., Skinner, G. K., & Grindlay, J. E. 2000, ApJ, 533, 329
Bazzano, A., Cocchi, M., La Padula, C., Sood, R., & Ubertini, P. 1993, A&AS, 97, 169
Belloni, T., Méndez, M., van der Klis, M., Lewin, W. H. G., & Dieters, S. 1999, ApJ, 519, L159
Bevington, P. R., & Robinson, D. K. 1992, Data Reduction and Error Analysis for the Physical Sciences (New York: McGraw-Hill)
Bisnovatyi-Kogan, G. S., & Blinnikov, S. I. 1977, A&A, 59, 111
Böttcher, M., & Liang, E. P. 1998, ApJ, 506, 281
Buck, R., & Lent, E. 1993, LLNL Energy and Technology Review (Livermore: LLNL)
Chen, W., Gehrels, N., & Leventhal, M. 1994, ApJ, 426, 586
Chu, Y., Kim, S., Points, S. D., Petre, R., & Snowden, S. L. 2000, AJ, 119, 2242
Cowley, A. P., Crampton, D., & Hutchings, J. B. 1987, AJ, 93, 195
Esin, A. A., McClintock, J. E., & Narayan, R. 1997, ApJ, 489, 865 (EMN)
Esin, A. A., Narayan, R., Cui, W., Grove, J. E., & Zhang, S. 1998, ApJ, 505, 854
Filippenko, A. V., Leonard, D. C., Matheson, T., Li, W., Moran, E. C., & Riess, A. G. 1999, PASP, 111, 969
Gilfanov, M., et al. 1993, ApJ, 418, 844
Grebenev, S. A., Pavlinsky, M. N., & Sunyaev, R. A. 1997, in The Transparent Universe, ed. C. Winkler, T. Courvoisier, & Ph. Durouchoux (ESA SP-382; Noordwijk: ESA), 183
Grindlay, J., et al. 2000a, in AIP Conf. Proc. 510, The Fifth Compton Symposium, ed. M. L. McConnell & J. M. Ryan (New York: AIP), 784
Grindlay, J., et al. (EXIST Science Working Group). 2000b, BAAS, 32, 2004
Harrison, F. A., Kahn, S. M., Hailey, C. J., Ziock, K. P., & Lubin, P. M. 1989, Proc. SPIE, 1159, 36
Heindl, W. A., & Smith, D. M. 1998, ApJ, 506, L35
Hua, X., & Titarchuk, L. 1995, ApJ, 449, 188
Iwan, D., Shafer, R. A., Marshall, F. E., Boldt, E. A., Mushotzky, R. F., & Stottlemyer, A. 1982, ApJ, 260, 111
Jung, G., Kurfess, J., Johnson, W., Strickman, M., Kinzer, R., Purcell, W., Grabelsky, D., & Ulmer, M. 1993, in AIP Conf. Proc. 304, The Second Compton Symposium, ed. C. Fichtel, N. Gehrels, & J. P. Norris (New York: AIP), 427
Keck, J. W. 2001, Ph.D. thesis, Columbia Univ.
Kuznetsov, S. I., et al. 1999, Astron. Lett., 25, 351
Liang, E. P. 1998, Phys. Rep., 302, 67
Liang, E. P. T., & Price, R. H. 1977, ApJ, 218, 247
Lin, D., Smith, I. A., Böttcher, M., & Liang, E. P. 2000a, ApJ, 531, 963
Lin, D., et al. 2000b, ApJ, 532, 548
Main, D. S., Smith, D. M., Heindl, W. A., Swank, J., Leventhal, M., Mirabel, I. F., & Rodríguez, L. F. 1999, ApJ, 525, 901
Maisack, M., et al. 1993, in AIP Conf. Proc. 304, The Second Compton Symposium, ed. C. Fichtel, N. Gehrels, & J. P. Norris (New York: AIP), 451
Mandrou, P. 1990, IAU Circ., 5032, 1
Martí, J., Mereghetti, S., Chaty, S., Mirabel, I. F., Goldoni, P., & Rodríguez, L. F. 1998, A&A, 338, L95
Méndez, M., & van der Klis, M. 1997, ApJ, 479, 926
Mereghetti, S., Belloni, T., & Goldwurm, A. 1994, ApJ, 433, L21
Mereghetti, S., Cremonesi, D. I., Haardt, F., Murakami, T., Belloni, T., & Goldwurm, A. 1997, ApJ, 476, 829
Mirabel, I. F., Cordier, B., Paul, J., Lebrun, F., & Duc, P. A. 1992a, IAU Circ., 5655, 1
Mirabel, I. F., & Rodríguez, L. F. 1993, in AIP Conf. Proc. 304, The Second Compton Symposium, ed. C. Fichtel, N. Gehrels, & J. P. Norris (New York: AIP), 413
Mirabel, I. F., Rodríguez, L. F., Cordier, B., Paul, J., & Lebrun, F. 1992b, IAU Circ., 5477, 1
———. 1993, A&AS, 97, 193
Narayan, R., Garcia, M. R., & McClintock, J. E. 1997, ApJ, 478, L79
Narayan, R., & Yi, I. 1995, ApJ, 452, 710
Predehl, P., & Schmitt, J. H. M. M. 1995, A&A, 293, 889
Rodríguez, L. F., Mirabel, I. F., & Martí, J. 1992, ApJ, 401, L15
Shapiro, S. L., Lightman, A. P., & Eardley, D. M. 1976, ApJ, 204, 187 (SLE)
Skinner, G. 1991, in AIP Conf. Proc. 232, Gamma-ray Line Astrophysics, ed. P. Durouchoux & N. Prantzos (New York: AIP), 358
Smith, D. M., Heindl, W. A., & Swank, J. H. 1999, IAU Circ., 7266, 2
Sunyaev, R., et al. 1991, in AIP Conf. Proc. 232, Gamma-ray Line Astrophysics, ed. P. Durouchoux & N. Prantzos (New York: AIP), 29
Tanaka, Y., & Lewin, W. H. G. 1995, in X-Ray Binaries, ed. W. H. G. Lewin, J. van Paradijs, & E. P. J. van den Heuvel (Cambridge: Cambridge Univ. Press), 126
Titarchuk, L. 1994, ApJ, 434, 570
Valinia, A., & Marshall, F. E. 1998, ApJ, 505, 134
Wilcox, T. P., J., & Lent, E. 1989, COG-A Particle Transport Code Designed to Solve the Boltzmann Equation for Deep-Penetration (Shielding) Problems (Vol. 1; Tech. Rep. M-221-1; Livermore: LLNL)
Zhang, S. N., Cui, W., Harmon, B. A., Paciesas, W. S., Remillard, R. E., & van Paradijs, J. 1997a, ApJ, 477, L95
Zhang, S. N., Mirabel, I. F., Harmon, B. A., Kroeger, R. A., Rodríguez, L. F., Hjellming, R. M., & Rupen, M. P. 1997b, in AIP Conf. Proc. 410, Fourth Compton Symposium, ed. C. D. Dermer, M. S. Strickman, & J. D. Kurfess (New York: AIP), 141
Życki, P. T., Done, C., & Smith, D. A. 1997, ApJ, 488, L113